Construction and Building Materials xxx (xxxx) 124797

Contents lists available at ScienceDirect

Construction and Building Materials

journal homepage: www.elsevier.com/locate/conbuildmat

An accelerated chloride threshold test for uncoated steel in highly resistive cementitious systems (hr-ACT test)

Sripriya Rengaraju, Radhakrishna G. Pillai

Department of Civil Engineering, Indian Institute of Technology Madras, Chennai, India

ARTICLE INFO

Article history:
Received 22 October 2020
Received in revised form 23 August 2021
Accepted 1 September 2021

Keywords:
Chloride threshold
Quenched and Self-tempered steel
Highly resistive cementitious binder
Limestone calcined clay cement

ABSTRACT

Currently, many supplementary cementitious materials are being used along with cement to reduce the CO_2 emissions. These cementitious systems exhibit very high resistivity due to pozzolanic reactions and the traditional test methods are inadequate to assess their durability performance related to corrosion, especially chloride threshold (Cl_{th}). This paper presents development of a test method (hr-ACT) for determining the Cl_{th} of such highly resistive systems with guidelines for identifying the same. The test specimen consisted of a mortar cylinder (lollipop) (cement:sand = 1:2.75) with steel embedded at the centre. Three binders, namely, OPC (w/b = 0.5), PC-FA (70% OPC + 30% Class F Fly ash) (w/b = 0.5) and Limestone Calcined Clay Cement (LC3 – 50% OPC clinker, 31% calcined clay, 15% limestone and 4% gypsum) (w/b = 0.4), and Quenched and Self-tempered (QST) steel were used in this study. The specimens were subjected to chloride in a cyclic wet-dry regime (2 day wet and 5 day dry) and the electrochemical impedance spectroscopy (EIS) test was conducted at the end of each wet period. Statistical analysis was done on the repeated polarization measurements (R_p) to detect corrosion initiation. Once corrosion initiation was detected, the total chloride content (acid soluble chlorides) in the mortar at the Steel–Cementitious binder (S-B) interface was determined using SHRP 330 and reported as Cl_{th}. The time required to complete hr–ACT test for an S–B system is about 3–4 months. The Cl_{th} was in the order OPC > PC–FA > LC3. Also, the synergistic effects of Cl_{th} and other parameters on service life are discussed.

1. Introduction

Reinforced concrete structures built with Ordinary Portland Cement (OPC) systems and located in marine environment can deteriorate prematurely due to inadequate chloride resistance. Fig. 1 shows the schematic representation of the service life of structures subjected to corrosion, where two distinct phases, namely initiation phase and propagation phase, are present. In case of chloride induced corrosion, the initiation phase is usually the longest phase in the service life of structures. If the cementitious matrix is not of good quality i.e., highly permeable, this phase is shortened and leads to shorter service life. Hence, nowadays, cements with pulverized fly ash (PC–FA), limestone calcined clay cement (LC3), etc. are used to enhance the resistivity against the ingress of moisture and chlorides and enhance the service life of concrete structures. However, Engineers need to assess the critical service life parameters of these highly resistive Steel–cementitious binder (S-B) systems in the short term (few months) – to assess if they are truly 'advanced' in enhancing the service life.

One of the critical service life parameters is the chloride threshold (Cl_{th}). Cl_{th} denotes the chloride concentration needed for corrosion initiation, and hence, estimation of Cl_{th} is necessary and important for estimating the service life of structures [2]. The estimation of Cl_{th} is very challenging because of its dependency on various factors such as (i) material properties of cover concrete, (ii) properties of steel reinforcement, and (iii) microclimate at the S-B interface [3]. The lack of consideration of these factors during the Cl_{th} testing can lead to erroneous and highly scattered results. Moreover, the electrochemical response from S-B systems depends on (i) the electrochemical technique used and (ii) the corrosion cell (configuration of specimen and electrodes) adopted. This dependency is due to variation of corrosion phenomena in different systems. Moreover, the cementitious cover could induce significant resistance (e.g., ohmic drop) during the electrochemical measurements [4]. The effect of this ohmic drop is of utmost importance while testing highly resistive S-B systems. However, authors could not find literature on ways to account for this during electrochemical tests on S-B systems. Also, ambiguity exists in identifying the highly resistive S–B system itself. The S-B systems develop resistivity over a period of time and de-

Department of Civil Engineering, Indian Institute of Technology Madras, Chennai, India

E-mail address: pillai@civil.iitm.ac.in (R.G. Pillai).

https://doi.org/10.1016/j.conbuildmat.2021.124797
0950-0618/

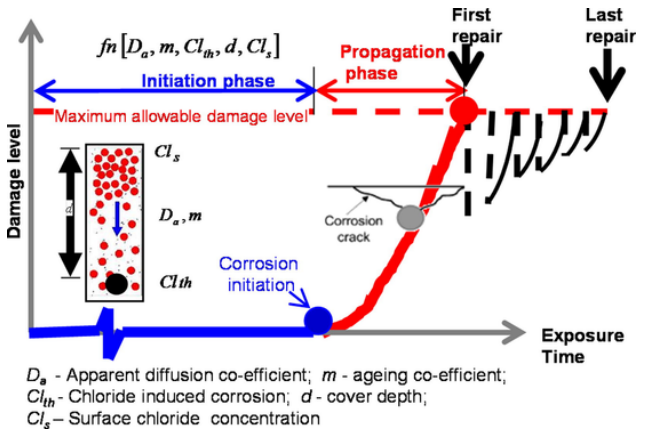

Fig. 1. Schematic showing various phases and factors affecting the service life (Tutti, 1982) [1].

pend on the w/b ratio, percentage replacement of OPC, age of curing, etc. Hence, there is a need to identify and define the highly resistive S–B system.

1.1. Effect of material properties on the Cl_{th}

A variety of cementitious binders with various SCMs are available, the use of which in concrete can affect the corrosion initiation in four ways. First, SCMs can enhance the pore size distribution of the hardened cement matrix by either the filler effect or secondary hydration reactions [5,6]. In general, a reduction in the mean pore diameter of the matrix can reduce the chloride ingress rate, which can delay the onset of corrosion. Second, SCMs consume OH^- ions during the secondary hydration reactions and increase the ionic resistivity [7]. The higher the concrete resistivity, the lower will be the ionic flow between anodic and cathodic regions; hence, lower corrosion rate [8,9]. Third, SCMs containing alumina improve the chloride binding capacity of concrete, thereby restricting the chloride ions from reaching the steel surface [6]. Fourth, the presence of SCMs can also lead to a reduction in the pH and the pH buffering capacity of concrete. This reduction in pH can influence the formation of the passive film and can reduce the Cl_{th}, which is a key parameter affecting the corrosion initiation [10]. In addition to the type of binder (composition and reactivity), the replacement level also plays a vital role in the Cl_{th} as the availability of $Ca(OH)_2$ at the S-B interface depends on replacement level of OPC [11,12]. Other factors, such as the type of steel and its surface finish and addition of corrosion inhibiting admixtures, also affect the Cl_{th}, but these are beyond the scope of this paper.

1.2. Effect of exposure conditions on the Cl_{th}

For obtaining corrosion results in the short term, various techniques are used to accelerate the access to chlorides at the S-B interface and/or corrosion process. The effect of these techniques on Cl_{th} are discussed in detail followed by the effect of the microclimate at the S-B interface on Cl_{th}. Then, the effect of chlorides on the formation of corrosion products is discussed.

1.2.1. Effect of techniques to accelerate ingress of chlorides on Cl_{th}

Techniques for accelerating the chloride ingress at the S-B interface include (i) immersion or cyclic wet-dry exposure using chloride solution, (ii) premixing the concrete with chlorides (i.e., admixed chlorides), and (iii) impressed current or potential gradient. When immersed in a chloride solution or when subjected to cyclic wet-dry exposure, the Cl^- ions accumulate at the S-B interface due to diffusion and/or capillary suction. This condition mimics the real field structures, and hence, the form of corrosion and the corrosion products are close to the realistic corrosion process [3]. However, this type of exposure (immersion or cyclic wet-dry) takes a long time to initiate corrosion in good quality concretes [13]. Also, different cyclic wet-dry regime will influence the transport of chlorides in different manner and hence, the time of corrosion initiation. Hence, researchers started assessing the corrosion performance of steel by embedding it in mortar instead of concrete. Even then, it takes several months to initiate corrosion when pozzolans and/or low w/b are used [14]. Hence, to bypass or shorten the test duration required for natural chloride ingress in good quality concrete specimens, researchers have either used admixed chlorides or impressed current. Admixed chlorides in fresh concrete can accelerate the cement hydration and change the morphological structure of C-S-H gel and lead to the formation of a non-uniform and weak passive film on the steel surface [15,16]. Hence, to accelerate the chloride ingress, an impressed current technique (by applying a constant potential gradient) was used by Trejo and Pillai [17]. However, the nature of the S-B interface can vary due to the application of the potential, especially for inhibitor systems with complex ions [18]. The application of potential induces the movement of nitrite ions along with the chloride ions to the S-B interface in case of nitrite-based inhibitors and neutralize the effect of chloride ions at the S-B interface. This neutralization effect results in increase of Cl_{th} than the realistic values in field conditions. Hence, application of potential is not suitable for finding the Cl_{th} in systems with complex ions. Hence, there is a need for developing a short-term test method using the cyclic wet-dry regime to determine the Cl_{th}.

1.2.2. Effect of micro-climate at the S-B interface

Corrosion initiation of steel depends on the physical and microclimate conditions of the S-B interface [3]. Major factors influencing the microclimate at the S-B interface are (i) moisture, (ii) oxygen, (iii) temperature, and (iv) pH conditions [19–21]. The microclimate depends heavily on the thickness and bulk properties of cover concrete and the exposure conditions. The formation of the passive film and the amount of chlorides needed for de-passivation depends on the microclimate [22]. Variation in the microclimate due to the exposure condition adopted during testing leads to variation in Cl_{th} [19]. This explains the huge scatters in the Cl_{th} values reported in the literature. Therefore, maintaining a known ambient condition and the timing of measurement throughout testing is essential.

1.3. Effect of the electrochemical technique used on the determined value of Cl_{th}

Even in traditional systems to determine Cl_{th}, Andrade (2016) reported that "…tests considering partial saturation or de-icing salts are not standardized…" [23]. Table 1 shows the widely adopted standard test methods used for assessing the corrosion of steel. However, some of the test methods have severe limitations when applied to S-B systems. Half-cell potential measurements can fluctuate due to moisture content, the resistivity of the cementitious matrix, cover thickness, the coating on the steel and the ASTM C876 cannot be adopted for all the exposure conditions [24–27]. In the ASTM G109 test method, the macrocell current between the rebar near to the exposure surface and the passive rebar at the farther end is measured. There is a possibility of the occurrence of corrosion with both anode and cathode on the same rebar (a top bar near to the exposure surface) when the resistivity of concrete is high [13,28].

Linear polarization resistance (LPR) is one of the advanced electrochemical techniques used to assess the instantaneous corrosion rate of steel in concrete. However, there is no standardized procedure to detect corrosion initiation. Also, the electrochemical reading is inclusive of the electrolyte resistance (concrete/mortar) (R_Ω) and is based on the assumption that the measured polarization value $R_p \gg R_\Omega$ [29,30]. For highly resistive cementitious systems, electrolyte resistance (ohmic drop) is not negligible. Also, the ohmic drop can distort the polarization

Table 1
Standard test methods for corrosion assessment of steel.

Methods	Electrolyte	Exposure Condition	Remarks
ASTM C876 – 2015 (Half-cell Potential) [33]	Concrete	Laboratory/ Field conditions	• Only for uncoated steel reinforcement • Initiation criteria: Half-cell potential < -350 mV vs CSE – 90% probability of corrosion
ASTM G109 – 2009 (Macrocell corrosion) [34]	Concrete	Wet-dry cycle (14w – 14 d)	• Only for uncoated steel reinforcement • Initiation criteria: Cumulative Current greater than 150 Coulombs (C)
ASTM G59 ASTM G5, ASTM G180, ASTM G102 (Polarization curves)[35–38]	NA	Immersion	• Cannot be used for electrolyte resistance of significant value • Cannot distinguish the corrosion mechanism of different steel types
ASTM STP 1506 (EIS) [39]	NA	Varied temperature	Can be used for performance evaluation of coated steels in aqueous systems
ASTM STP 1188 (EIS) [40]	NA	NA	Can be used for performance evaluation of coated steels in highly resistive media
JIS A 6205 [41]	Concrete	180 °C, 1 Pa, Saturated water vapour	For evaluating corrosion inhibiting admixtures in concrete

curve as well as the input scan rate, which could influence the measured R_p. The current interruption technique is essential to overcome this effect [31]. In many cases, due to specimen geometry, the current interruption may not yield a good response. In such cases, a testing technique that accounts for the performance of the individual component in an advanced S-B system technique is useful. Electrochemical Impedance Spectroscopy (EIS) is one such technique that can yield more information about the reaction kinetics at the S-B interface by separating individual components' responses. However, a deep understanding of the system and the relevant electrical parameters are necessary for analysis. There are also severe challenges in formulating a suitable equivalent circuit, especially for advanced S-B systems [32].

1.3.1. Initiation criteria

The next important aspect of Cl_{th} is the initiation criteria adopted to detect corrosion initiation. The initiation criteria greatly influence the reported Cl_{th} as different systems respond differently for the adopted test method due to the specimen geometry, resistivity, etc.

Table 2 shows the different approaches to initiation criteria for detecting corrosion initiation.

Figure 2 shows the graphical representation of the time interval taken to reach the initiation criteria on the same specimen when different approaches are adopted (interpreted by the author based on the literature mentioned in Table 2). Thus, the initiation criteria adopted induces significant scatter in the reported Cl_{th} values.

Given this scenario, the suitability of the existing electrochemical techniques and Cl_{th} test methods (for conventional S-B systems) to the highly resistive S-B systems needs to be assessed. Also, guidelines to i) select an appropriate technique and test method, ii) acquire quality electrochemical response data, and iii) interpret such data from highly resistive S-B systems are not available. This makes it difficult to detect

Table 2
Review of approaches to detect corrosion initiation in steel-cementitious binder systems.

Initiation Criteria	Reference
Significant weight loss from certain exposure time	[42]
Fixed OCP (E_{corr} < -350 mV Vs. CSE)	[33,43–45]
Fixed charge passed (Q greater than 150 Coulombs)	[34]
Fixed polarisation resistance (R_p less than 10,000 Ω.cm^2)	[46]
Fixed current density (i_{corr} greater than 0.1 μA/cm^2)	[27,47,48]
Sudden increase/decrease in corrosion parameter (OCP, R_p/i_{corr}, Current required for maintaining potentiostatic control)	[49–52]
Statistically significant change in the corrosion parameter	[17,18]

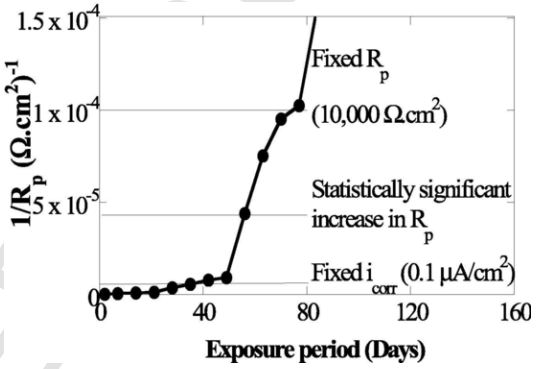

Fig. 2. Effect of corrosion initiation criteria on Cl_{th}.

the initiation of corrosion of steel embedded in systems with highly resistive binders. Hence, there is a need for a short-term test method for estimation of Cl_{th} of steel in highly resistive binder systems.

2. Research significance

Major infrastructure projects are designed for 100 + years. Many materials come into the market claiming low cost, constructability, sustainability, and durability. There is a need to assess the material behaviour, especially the chloride threshold (Cl_{th}), to ensure the claimed performance. Traditional test methods available for S-B systems were developed for concretes with low-to-moderate resistivity. Even after decades of research work, there is no clarity about the test method and technique to be used for determining the Cl_{th} of highly resistive steel-binder systems. Also, there are no clear guidelines for data acquisition and interpretation during the assessment. This paper gives guidelines for identifying highly resistive binder systems and a test method (hr-ACT) to determine the Cl_{th} in such systems.

3. Methodology

A comprehensive experimental program was conducted to determine the Cl_{th} of the highly resistive S-B systems. Three types of binders, namely Ordinary Portland Cement (OPC), 70% OPC and 30% Class F fly ash (PC-FA), and the LC3 system consisting of 50% OPC clinker, 31% calcined clay, 15% limestone and 4% gypsum were used for the study. Quenched and self-tempered (QST) steel (known as thermo-mechanically treated (TMT) steel in the Indian sub-continent) rebar embedded in these binder systems were used to determine the Cl_{th}.

3.1. Specimen preparation

The steel specimen (8 mm diameter) of length 100 mm is cut using a coolant to ensure that the edges of the rebar are free of heat affected zone. The cut ends of the steel are ground to have a smooth finish with-

out any sharp edge. A 4-mm thread was done by means of drilling and threading at the center of the 8 mm diameter steel rebar. The rebar is cleaned using an ultrasonic cleaner with the help of mild reagent ethanol until no visible rust products are seen. A stainless steel fully threaded rod is screwed to the 8 mm rebar. Neoprene tube of sufficient thickness is used to seal the junction of stainless steel and steel rebar to prevent galvanic corrosion. Mortar (cement:sand = 1:2.75) is prepared and the lollipop specimen is cast as shown in Fig. 3. For OPC and PC-FA specimens, w/b of 0.5 was chosen whereas LC3 mix had w/b of 0.4. The w/b of LC3 was chosen to a lower value of 0.4 to match the resistivity of LC3 mix produced in the first industrial trial production.

The specimen is demoulded using a hot air blower and the bottom conical portion is dipped in epoxy bath (small conical plastic cup with epoxy) to ensure a thicker coating to avoid corrosion due to the smaller cover thickness and left to cure in laboratory environment (25 °C and 95% RH approximately) for 28 days. After 28 days of curing, the external surface of the mortar specimen is epoxy coated (two coat) leaving 50 mm at the middle as shown in Fig. 3. The specimens are subjected to the cyclic wet-dry regime [2 days wet and 5 days dry (2W-5d)] in simulated pore solution (SPS) with 3.5% NaCl (relative to that of solution) in the standard laboratory conditions (25 °C and 65% RH approximately). SPS contained 10.4 g of NaOH, 23.2 g of KOH, 0.3 g of $Ca(OH)_2$, in 966 g of distilled water [53]. The pH of SPS is similar to that of cementitious system under testing and is used to avoid leaching of compounds such as $Ca(OH)_2$.

3.2. Corrosion test set up

The workstation (Solartron 1287 Potentiostat coupled with Solartron 1255 Frequency response analyser), and a 3-electrode corrosion

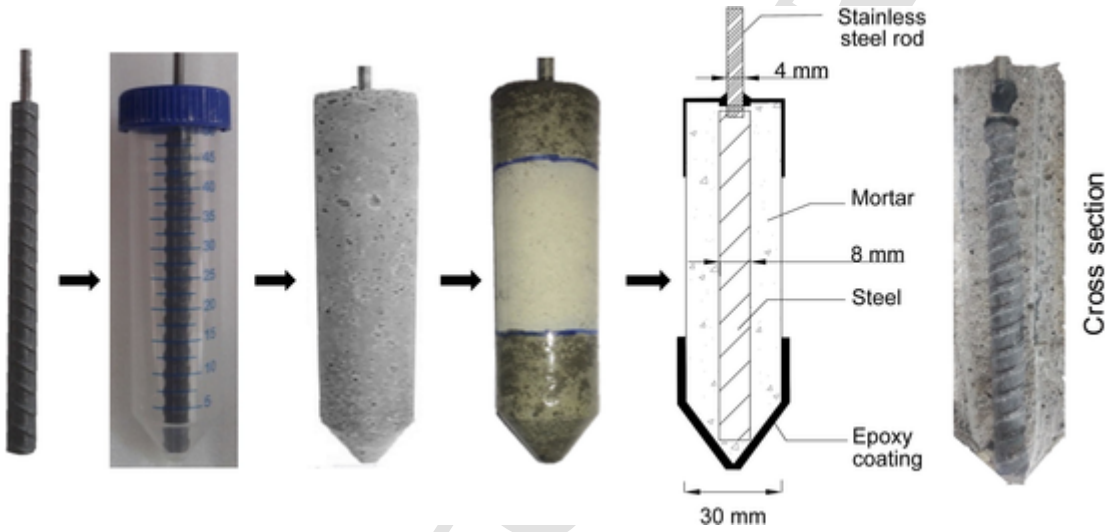

Fig. 3. Lollipop casting – step-by-step procedure and cross section.

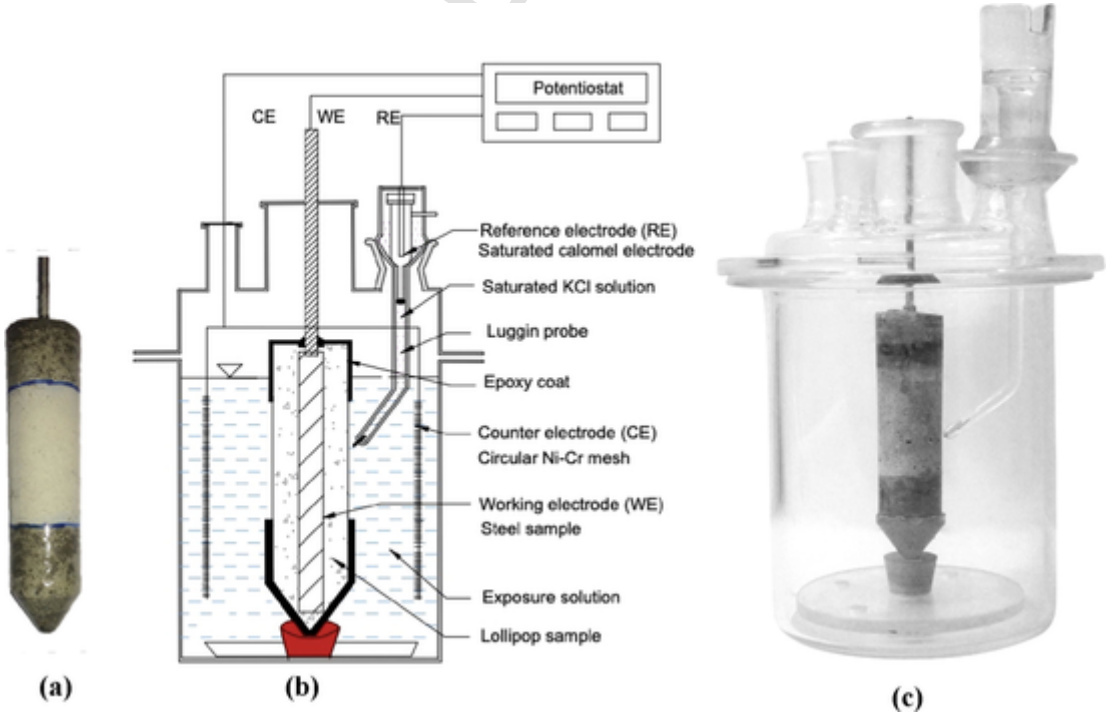

Fig. 4. Shows a schematic diagram of the corrosion test setup used in this study. (a) Lollipop specimen, (b) Schematic of corrosion cell set up and (c) Photo of corrosion cell (Counter electrode excluded for clarity).

cell setup (working electrode (WE), counter electrode (CE), and reference electrode (RE)) as shown in Fig. 4 were used to conduct the Electrochemical Impedance Spectroscopy (EIS) test. The middle region (50 mm) of the steel piece, which is directly exposed to chlorides through uncoated mortar was considered as the WE. A 90 mm diameter pipe made of Nichrome wire mesh was used as the CE. The test specimen was placed inside this CE. The saturated calomel electrode (SCE) was used as the RE and placed close to the surface of mortar. All the electrodes were placed in a glass beaker with SPS + 3.5% NaCl solution. This corrosion cell setup was then connected to the workstation and computer for recording the readings.

3.3. Monitoring of electrochemical response

The specimen was subjected to cyclic wet-dry regime [(2W-5d)] and at the end of the wet period, electrochemical measurements were taken. At first, the Open Circuit Potential (OCP) of the steel specimen was measured. Immediately after measuring the OCP, EIS was monitored. The EIS response was recorded by oversiding a perturbation signal of ± 10 mV (peak-to-peak) amplitude at OCP and by sweeping the frequency from 100 kHz to 0.01 Hz. The data was collected at 10 points per decade. Once the EIS response was collected, the R_p of steel was calculated by fitting an equivalent circuit (see Fig. 5). The procedure for fitting the equivalent circuit is explained later. After obtaining the EIS response, LPR data were also collected at a scan rate of 0.05 mV/s and scan range of ± 10 mV from the OCP. These data were collected to understand the effect of techniques employed on the corrosion detection.

3.4. Initiation criteria

The methodology for hr-ACT is shown in Fig. 6 as a flowchart. A statistical corrosion initiation criterion was adopted where a stable set of five consecutive readings of $1/R_p$ were identified, in which each of the readings fell below the mean + 1.5 times the standard deviation (μ_{st} + 1.5σ_{st}). Once the stable data were identified, the specimens were continued with the monitoring till $1/R_p$ crosses the value of mean + 3 times the standard deviation (μ_{st} + 3σ_{st}) at which the specimen was considered to have initiated corrosion. This 3σ criterion was developed based on a detailed statistical analysis of time versus inverse polarization resistance ($1/R_p$) data of various test specimens and is given in Karuppanasamy and Pillai [18]. It was observed that the σ and 2σ were not successful in detecting corrosion initiation because of the large scatter in the $1/R_p$ data, which is very common in such corrosion experiments of steel in a sol–gel cementitious system [54]. Moreover, 3σ criteria was able to overcome this challenge and was adopted in this work.

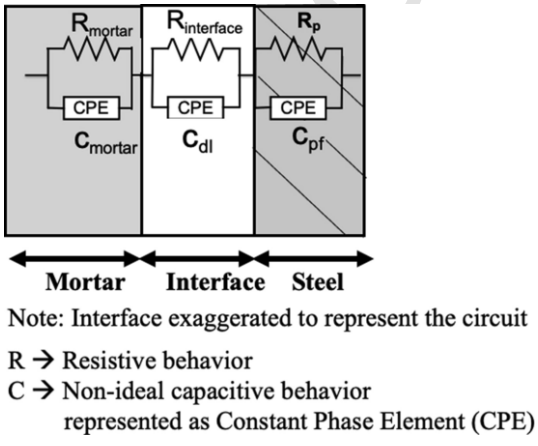

Fig. 5. Physical components representing the individual elements of the chosen equivalent electrical circuit (EEC).

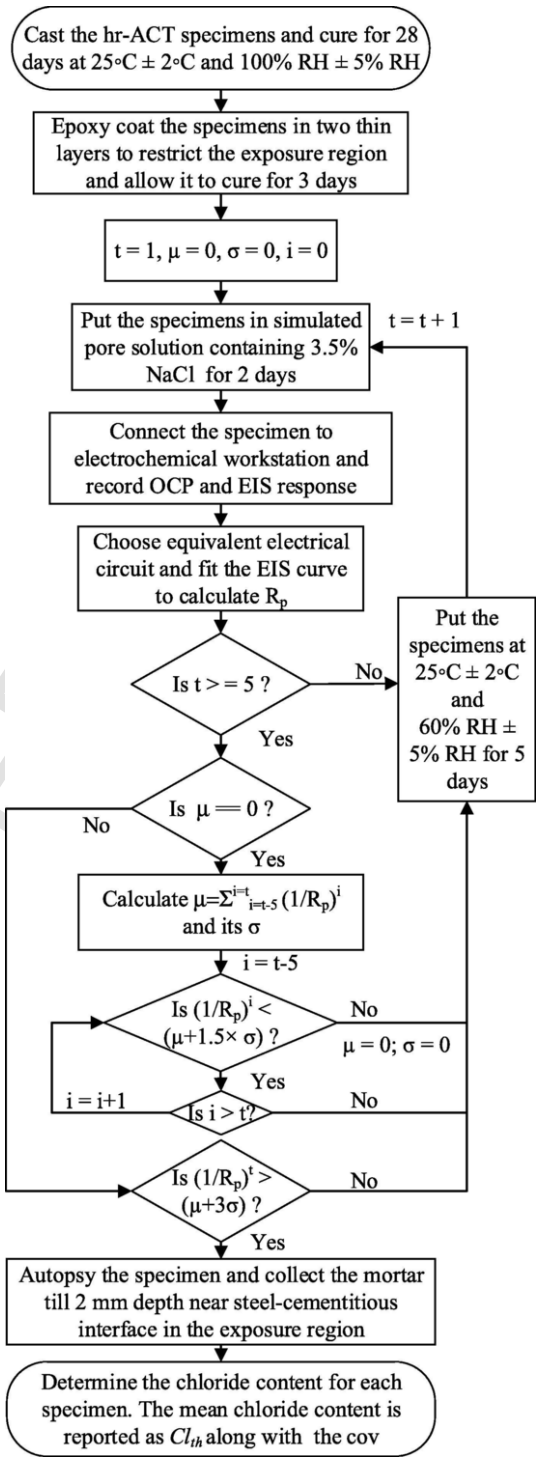

Fig. 6. Flowchart showing step by step procedure for hr-ACT test method.

Fig. 7 shows a typical inverse polarization data curve with the stable data and corrosion initiation point marked.

3.5. Characterization of pit by tomography

After the corrosion initiation is detected by electrochemical reading, the specimen is autopsied such that the specimen is split into two halves. The steel rebar is extracted and visually observed for the corrosion spots. Then, the steel rebar is wire brushed and wiped clean with a cotton cloth and sent for X-ray Computed Tomography X-CT. A power source of 150 kV had been used for the scan. The images were taken us-

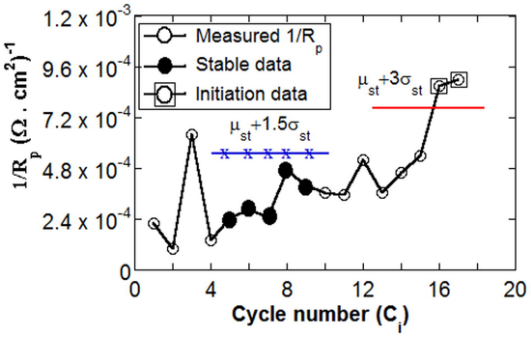

Fig. 7. Graph showing the stable data and the initiation point.

ing the following parameters (a) current of 150 mA, (b) exposure time of 333 ms and (c) resolution of 115 μm. The obtained images were then reconstructed to 3-D image of the steel rebar using VG studio max 22.6. The sliced images were analysed using Matlab™ for corrosion pit depth.

3.6. Cl_{th} analysis in the mortar at S-B interface

The lollipop specimens were autopsied, and the mortar powder was collected from the S-B interface. The acid soluble chloride content was found using SHRP 330 method [55]. Here, the Cl_{th} is taken as acid soluble chlorides and not the water-soluble chloride. The bound chlorides can be released anytime due to other deterioration mechanisms such as carbonation of the cover concrete, where the pH of the concrete reduces. Hence, this study focused on determining acid soluble chlorides. Also, this will give a conservative value of Cl_{th} – a safer approach according to ACI 318–19 section 26.4.2.2 [56].

4. Results and discussion

The definition of a highly resistive cementitious system is presented, followed by the discussions on the test method where the lollipop specimens with three binders, namely OPC, PC-FA, and LC3, were subjected to the cyclic wet-dry regime, and the polarization resistance was monitored. The effect of binders and chloride exposure on the EIS spectra, the explanation of the electrical equivalent circuit, how to fit the EIS curve, and initiation criteria are explained in detail. Further, discussions on the effect of resistivity on the electrochemical response, tomography analysis and the determination of Cl_{th} are also presented.

4.1. Highly resistive cementitious systems

The resistivity development is a key factor in the electrochemical response indicating chloride induced corrosion. However, there are no guidelines available for determining what constitutes the 'highly resistive' concrete systems for which ohmic drop should be considered during electrochemical measurements. Hence, this study adopted the AASHTO T 358 (2017), where the chloride resistance of concrete is correlated with its surface resistivity measured using Wenner 4–probe resistivity meter [57]. According to this, any cementitious system having a surface resistivity more than 37 kΩ.cm has 'high' chloride resistivity (irrespective of its formulation, w/b, and age). In this paper, a similar classification, where the surface resistivity of concrete greater than 37 kΩ.cm, is considered as a 'highly resistive cementitious system'. The experiments leading to the adoption of such classification, where traditional test methods may not work is explained in Rengaraju et al. [54]. Fig. 8 shows the range of resistivity developed by concrete with different SCMs and w/b [58–61]. It should be noted that not all the SCM-based concretes exhibit 'high' resistivity and there is a scatter in the resistivity values reported, especially in the concretes with fly ash or slag. This is due to their slow reactivity, w/b, replacement level and age of

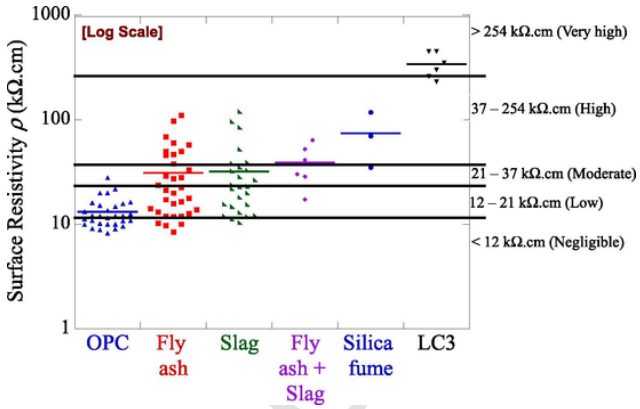

Fig. 8. Surface resistivity of concretes made with various binders [categories are as per AASHTO T 358 (2017) [57–61]].

the concrete at the time of testing (say, 28 days). So, all the SCM-based concretes may not be highly resistive. Also, it should be noted that the resistivity of all OPC concretes were lower than 37 kΩ.cm – indicating low resistivity, which do not have significant ohmic drop and associated difficulties during electrochemical measurements.

4.2. Effect of binders and chloride exposure on the EIS spectra

Figure 9 shows typical EIS curves for OPC, PC-FA, and LC3 systems when exposed to chlorides. The EIS spectrum is placed in the Nyquist plot depending on the type of binder, w/b, and the age of the specimen at the time of testing. The spectrum shifts away from the origin as the resistivity of the mortar cover increases. In systems with early hydration reactions such as OPC, LC3, etc., the EIS spectra of the specimens will be away from the origin in the Nyquist plot when the initial reading is taken at 28 days of curing and will not shift any further. When the specimens are exposed to chlorides, the resistivity reduces, and the curve starts moving towards the origin. In the case of PC-FA, as the hydration reaction progresses, the EIS curve will slowly move away from the origin, showing an increase in resistivity. However, the increase in resistivity of the mortar due to hydration in PC-FA will be counterbalanced by the ingress of chlorides and the position of the EIS curve will be the net effect of the two depending on the age of the specimen at the time of chloride exposure. Hence, different binders have a different effect on the position of EIS curve. The shift of the EIS curve is also dependent on the duration of exposure. If the specimen is not sufficiently saturated before the testing, the curve will show an increase in resistivity. This also explains the need for testing at the same time of exposure each time.

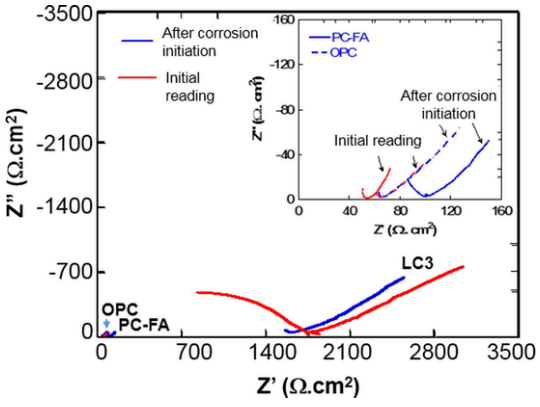

Fig. 9. Effect of binders, age and chloride exposure on the EIS spectra.

4.3. Details of the equivalent circuit

Figure 5 represents the equivalent electrical circuit (EEC) for obtaining the polarization resistance from the EIS spectrum. The EEC should represent the physical components of the specimen and the underlying reactions, and hence depend upon the nature of the specimen and its exposure condition. This EEC is particularly useful when the steel is uncoated and the specimen is subjected to chloride induced corrosion. The EIS spectrum consists of three major components, which arises from the physical segments present in the specimen (See Fig. 5). The first component represents the properties of the cover mortar. Since the mortar is a non-homogenous porous medium, it is represented by resistor and non-ideal capacitor in parallel. The second segment is the S-B interface. Again, this is also represented by resistor and non-ideal capacitor in parallel because of its porous nature. The S-B interface is more porous compared to the bulk cover and hence, the resistance offered by this component is lower compared to the bulk cover. The third component characterizes the steel with a passive film. Hence, the resistor represents the polarization resistance of the steel, which is in parallel with the non-ideal capacitance. This non-ideal capacitance marks the porous nature of the passive film. When the steel is embedded in highly resistive systems like LC3, the resistivity of all the three components is high. The pore structure (finer pores) and associated tortuosity lead to greater deviation of the tail from 45° and hence, Warburg Impedance (used for indicating the diffusion tail at 45°) may not be applicable for these kind of highly resistive systems [62]. So, instead of Warburg impedance as the circuit element, CPE was used as a common component that can capture the effect of any binder on diffusion phenomena. In other words, the use of CPE eliminated the need for different EECs for concretes with different binders. Hence, the same EEC was used for data analysis after consideration of the process and components involved. The next step is obtaining the polarization resistance by fitting the circuit to the EIS spectrum.

4.4. Fitting the equivalent circuit

Before fitting the equivalent circuit, the correctness of the EIS curve should be tested. Since EIS spectra are prone to artefacts (i.e. distortions) from the surrounding environment, it is recommended to check the spectra before obtaining the values from the circuit using the Kramer-Kraig transform (KKT). The KKT transform will check the linearity of the spectra and establish the validity that the curve was obtained as the response to the input signal [63,64]. Once the curve is validated, the equivalent circuit can be formed in the fit optimization software that comes with the corrosion testing equipment. In this study, ZPlot® software, which comes with Solartron was used. For optimal fitting of the equivalent circuit, initial values can be fed. For e.g., the resistance of the mortar cover can be fed as the value, where the EIS curve dips (See Fig. 9(c) – around 1800 Ω.cm^2 in the initial curve of LC3) near to the real component of the Nyquist plot. After trial and error, the software will generate the optimum values for each of the component in the equivalent circuit. The values having the best fit with the experimental curve are treated as the solution. Since there are multiple components and the values are obtained after optimization, more than one solution is possible. To avoid error in interpretation, the following precautions can be taken, namely (i) the chi-squared value of the equivalent circuit should be less than 0.001, (ii) the error of the individual components should be less than 20%. [Usually, for metal-aqueous system, the error of the individual components is less than 5%. Here, the mortar and the S-B interface are of non-homogeneous nature and hence, some allowance should be permitted while fitting] and (iii) the power 'n' in the capacitance value calculation cannot be greater than 1 as it has no physical meaning. The capacitance value can be either pico- or nanofarad. While the above precautions are taken, the resistance of the third component can be considered as the polarization resistance of the steel. Fig. 10 represents the typical fit of the chosen EEC for the specimen under study (LC3 -S1 specimen)

4.5. Statistical initiation criteria

Since there is a search for sustainable low CO_2 materials as supplements, new materials with high resistivity are coming onto the market and the initiation criteria based on fixed absolute numbers might not work as mentioned in Fig. 2. If the cementitious system is highly resistive, there will a large ohmic drop and there will be distortion in the measurements. The resistivity of the cover may mask the undergoing corrosion and hence, the corrosion initiation may not be detected timeously. This delay in identifying the corrosion initiation will lead to false prediction of service life and can lead to erroneous judgment, causing premature failure of reinforced concrete structures. Also, if there is a coating or galvanization, or addition of corrosion inhibitors into the concrete, the interface is modified, and the surface of the steel has higher resistivity, and the fixed criteria may not work. So, there is a requirement that the initiation criteria should be based on a statistical evaluation of the previous readings of the same specimen rather than the fixed absolute numbers. Hence, in this study, a statistically based initiation criterion was adopted where a stable data was identified, in which the $1/R_p$ readings of five consecutive measurements were within $\mu_{st} \pm 1.5\sigma_{st}$. The stable data criterion ($\mu_{st} \pm 1.3\sigma_{st}$) adopted by Karuppanasamy and Pillai [18] was slightly modified for the EIS data as this R_p value is obtained from the optimization of the best fit and the values obtained after fitting will be closer to the previous readings unless there is significant corrosion.

4.6. The electrochemical response

Figure 11 shows the electrochemical response obtained using LPR and EIS techniques. The hollow circular marker represents the LPR

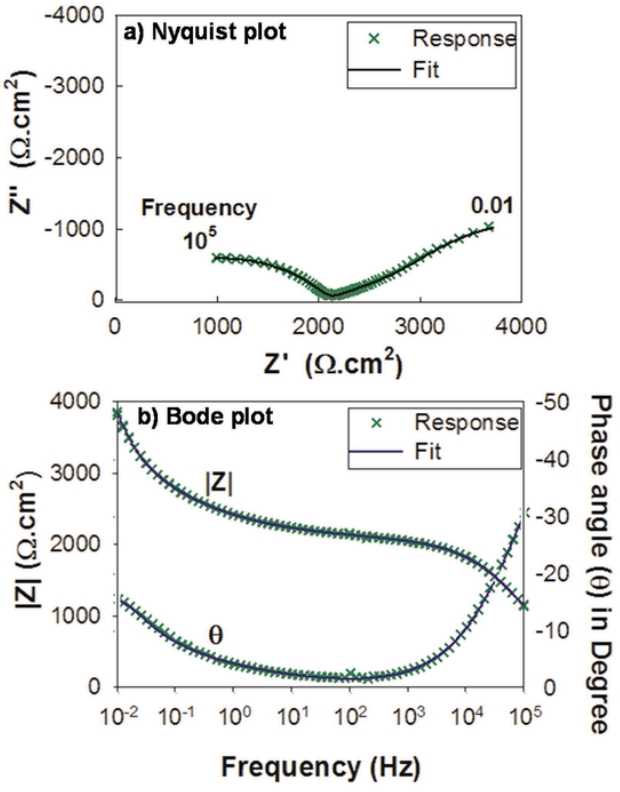

Fig. 10. EIS curve and its equivalent circuit fit.

reading, whereas the hollow square marker represents the EIS data. The stable data is represented as filled markers in both these techniques and was identified as mentioned earlier in Section 3.4. The mean and standard deviation of the stable data, μ_{st} and σ_{st} are calculated and kept as reference for detecting the corrosion initiation point. Then the electrochemical monitoring is continued till the reading $1/R_p$ reaches a value higher than $\mu_{st} + 3\sigma_{st,}$ where the specimen is considered to be initiated in corrosion. In Fig. 11, the initiation value is represented by big hollow squares superimposed on the existing hollow markers. Moreover, the steel specimen extracted at the time of corrosion detection is presented next to the electrochemical data.

In OPC and PC-FA specimens, due to lower resistivity of cover in the early ages of testing, LPR and EIS techniques did not have a significant variation in the corrosion initiation time. In OPC specimens, both LPR and EIS techniques detected corrosion initiation in the same number of cycles for all the specimens. In PC-FA specimens, some of the specimens (S2, S4, and S5) had one cycle delay in the detection of corrosion initiation using LPR when compared to EIS. However, this is not the case with highly resistive LC3 systems. There is a significant delay in the detection of corrosion initiation when LPR technique was used due to the high resistivity of the mortar cover.

The steel specimens from OPC and PC-FA systems indicate that the rust spots were superficial, the pit depth was not evident, and the region of corrosion initiation was scattered. This is due to the low resistivity offered by these systems for ionic conduction. However, the pit depth was significant in the case of highly resistive system as the path of ionic conduction is restricted due to the high resistivity.

The resistivity plays a major role in resisting the transport of chloride ions to the steel surface. There is a linear correlation between electrical resistivity and the chloride ion transport [65]. The ionic resistivity of the cementitious system (C-S-H and C-A-S-H gel), refined pore structure, less ions in the pore solution for ionic exchange (less alkalis in the pore solution) are some of the reasons for the delayed ingress of chloride ions in the high resistive systems [3,4]. However, due to this resistivity, there will be a significant ohmic drop in the measurement of electrochemical response and the measured electrochemical response may be distorted leading to misinterpretation of the ongoing corrosion process. Therefore, the testing techniques and data interpretation such as initiation criteria play major role in detecting the corrosion initiation in such highly resistive cementitious system. Also, the Cl_{th} obtained from two different testing techniques may not be similar as the electrochemical response may have significant variation due to the mode of acquisition.

Ideally, LPR and EIS should give similar electrochemical response when the electrolyte resistance (mortar resistivity) is negligible as in the case of metal-aqueous systems. LPR is one of the preferred techniques due to its simplicity and time-efficient data acquisition. As discussed earlier, LPR technique gives the total response of the system (mortar, interface and steel) and works perfectly for low resistive mortar cover such as OPC systems [66]. However, as the electrolyte resistance becomes very high or the system becomes complex with multilayered physical components such as mortar, S-B interface, coating on the steel, etc., it is necessary to account for each of the components in the electrochemical response for correctness in the data interpretation. Also, one may argue that the LPR with the current interruption technique works in these cases of high electrolyte resistance. However, the authors could not acquire a good response in the corrosion cell designed for this study with the chosen input parameters. Further details on the selection of the input parameters can be found in Rengaraju et al. [54]. In this study, only the LPR technique without current interruption was employed and EIS and LPR data were compared. Further to substantiate the claim that EIS detects the corrosion earlier, the pit depth was characterized by tomography.

4.7. Characterization of pit by tomography

Figure 12 shows the longitudinal-section of tomographic image of the corrosion pits observed in LC3 specimens when autopsied. Compared to low resistive systems, the pit depth was significant in case of LC3. There were no corrosion spots on other portions of the steel rebar in LC3 whereas the corrosion spots were more scattered over the initiation region in OPC and PC-FA systems as mentioned earlier. A cross sectional loss as high as 4% at some sections of the rebar (S1 and S4) was observed, indicating a deeper pit in case of LC3. This kind of deep pit forms over time rather than a single exposure cycle indicating that the data acquisition using EIS technique is necessary in case of highly resistive cementitious systems.

4.8. Cl_{th} analysis in the mortar at S-B interface

Figure 13 shows the Cl_{th} values obtained from literature for OPC and from hr-ACT test method for the OPC, PC-FA, and LC3 binders respectively. The highest mean value of Cl_{th} is obtained for OPC (i.e., 0.4% by weight of binder) followed by PC-FA and LC3 systems, which is in the same order as that of their alkalinity (pH of the system) [10]. It is to be noted that the mean value for LC3 is lower than that for OPC and PC-FA, and hence, it creates an illusion that scatter for LC3 is insignificant. The chloride-induced corrosion produces hydrochloric acid as an intermediate product, which reduces alkalinity. To compensate the alkalinity at the interface, $Ca(OH)_2$ dissolution takes place and OH^- ions moves towards the sites of reduced alkalinity. This buffering action will take place depending on the availability of $Ca(OH)_2$. In the highly resistive SCM systems, the buffering action will be less as they consume $Ca(OH)_2$ during the early age of the hydration for the pozzolanic reaction. This action results in a lower pH in the pore solution and reduces the buffering capacity at the S-B interface compared to the conventional OPC system. When the chloride ions reach the steel surface and alter the passive film in the vacancy, there is a further drop in pH, leading to lower Cl_{th} in S-B systems with SCMs. Hence, highly resistive SCM-based systems lead to deeper pits, and the corrosion spots are more concentrated when compared to the less resistive concrete systems. So, the corrosion initiation must be detected as early as possible in such highly resistive SCM systems .

4.9. Synergistic effect of Cl_{th} and D_a on service life

It is to be noted that whenever OPC is replaced with SCM-based concretes, the Cl_{th} can reduce. However, lower Cl_{th} does not always indicate shorter service life. Due to the compact microstructure and high ionic resistivity for the ingress of deleterious agents in SCM-based concretes, their diffusion coefficients (D_a) are usually less than that of OPC systems. Therefore, the adverse effects on service life due to reduced Cl_{th} is compensated by the reduction of D_a in SCM based concretes. This can be illustrated by an example here. Consider a bridge deck of 50 mm cover with a concrete of strength 30 MPa. To calculate the service life, the following parameters are important, namely Cl_{th}, D_a, and m (i.e., ageing co-efficient - the effect of hydration on the microstructure of concrete as the concrete ages). Table 3 gives typical values of these properties (obtained from literature) for various low and highly resistive binders. This data set is then used to estimate the service life in Life-365™ software [74]. The estimated values of service life clearly show that the usage of highly resistive binders with low D_a enhances the service life in spite of their effect on lowering the Cl_{th}. For example, the first row with OPC system exhibits a life of about 7 years and the second row with fly ash exhibits a life of 29 years - an increase by 3 times. This is primarily due to the synergistic effect of Cl_{th} and D_a. Therefore, to enhance the service life, the usage of SCMs in concrete is recommended and it is highly recommended to evaluate the effect of

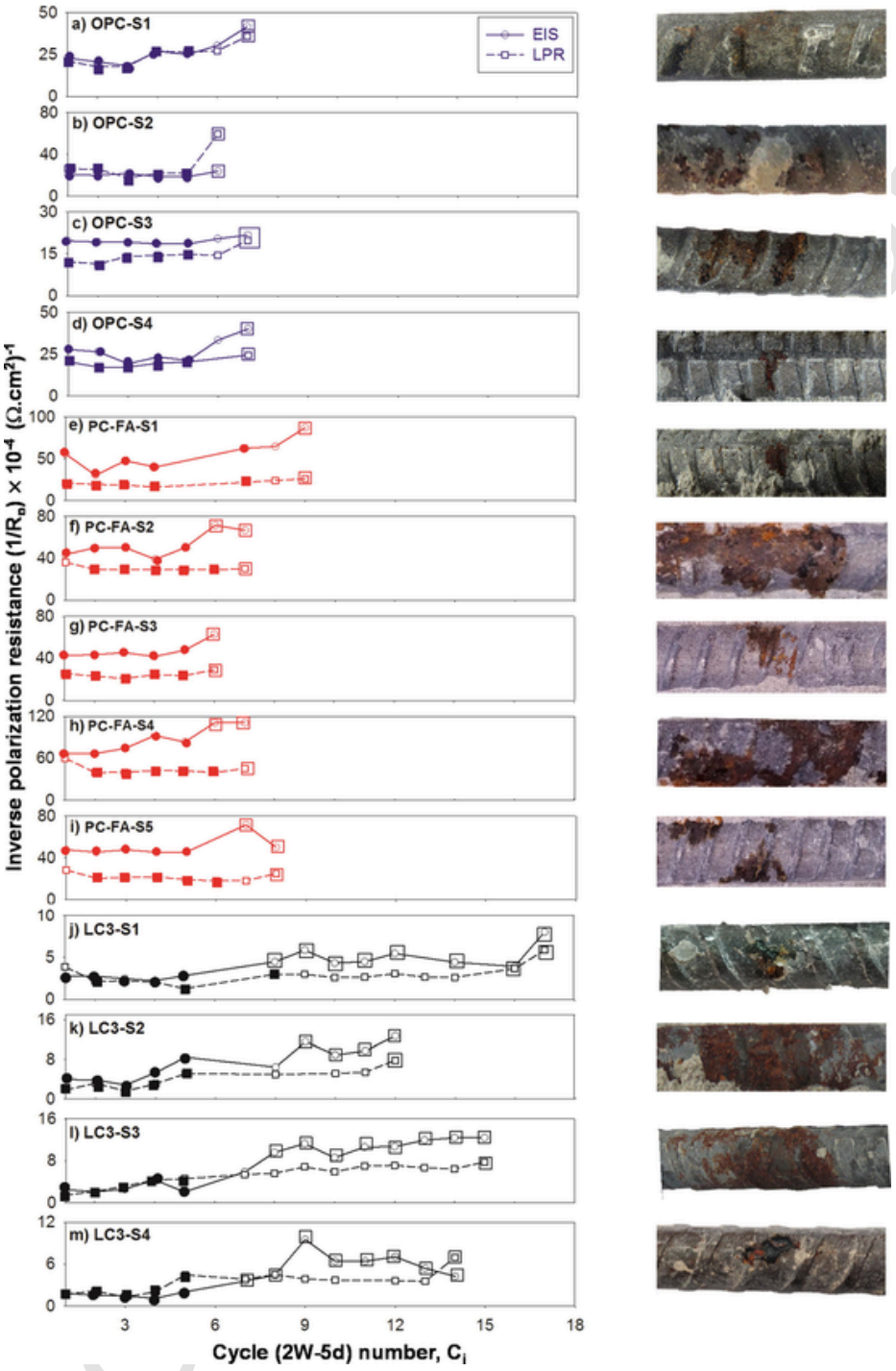

Fig. 11. Electrochemical response from EIS and LPR techniques and visual observation from OPC [w/b = 0.5], PC-FA [w/b = 0.5], and LC3 specimens [w/b = 0.4]

Cl_{th}, D_a, m, and cover depth while choosing a steel-cementitious binder system. Note that the values given in Table 3 are for the purpose of demonstration of this concept and can change as a function of mixture proportions.

4.10. Precautions to be taken during the hr-ACT test

The following precautions are recommended while conducting hr-ACT test.

- Specimen preparation: It is the crucial step in any corrosion related experiments and should be given the utmost importance. The steel specimen should be ensured that the portion under the ribs are clean and no visible corrosion spots on the steel are present. The lollipop specimen has very low cover at the bottom due to its conical nature and corrosion might start from there due to moisture. Sufficient care should be taken while casting the specimen leaving enough cover at the bottom. Also, once demoulded, the specimen should be thoroughly checked for honeycombs and other defects, and epoxy coated at the designated portions before subjecting it to chloride exposure.
- Specimen validation: The quality of the specimens should be validated before taken for continuous monitoring. The resistivity of the cover mortar in the initial reading (with the same steel type and

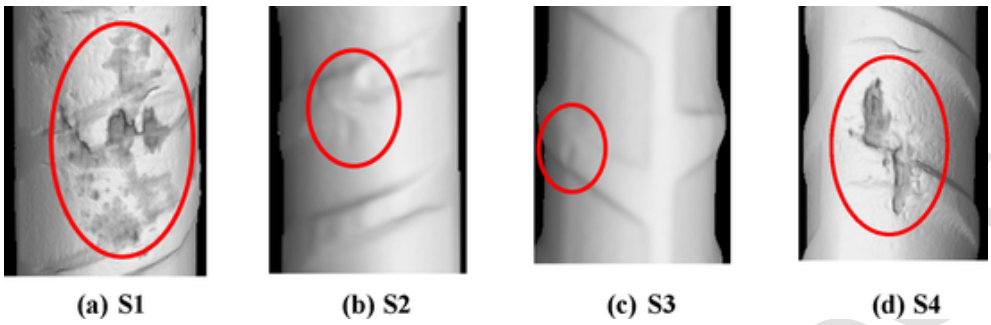

Fig. 12. Image of the pits captured by tomography in LC3 specimens.

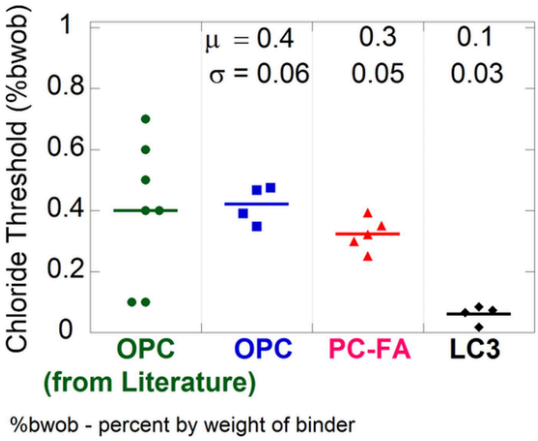

Fig. 13. Cl_{th} **for corrosion initiation of the rebar in OPC, PC-FA, and LC3 mortar compared with literature** [67–73].

Table 3
Service life estimation from Life-365 ™ for different binders (cover depth = 50 mm).

Example of binder type	Cl_{th}(% bwob)	D_a(×10^{-12} m^2/s)	m	Estimated service life (in years)	Percent increase in service life
Ordinary Portland cement (OPC)	0.4	25	0.4	7	Control case
Fly ash	0.3	5	0.55	29	300%
OPC + Slag	0.3	5	0.55	29	300%
OPC + Fly ash + Slag	0.2	5	0.6	28	300%
OPC + Silica fume	0.1	3	0.4	15	100%
LC3	0.1	3	0.5	23	200%

* % bwob – percentage by weight of binder.

binder type) should be around ± 30% of the value and should not be greater than 50% value obtained from other specimens in the same group. Hence, it is recommended to cast extra specimens for arriving at the required number of specimens (say, around 10 specimens).

- Monitoring: The specimens should be subjected to the cyclic wet dry regime (five days dry and two days wet) in a strict manner before taking the measurements. As the EIS spectra is prone to artefacts (distortions), it should be checked for the correctness of the data before further analysis.
- Equivalent electrical circuit: The equivalent electrical circuit given in this paper is applicable for lollipop specimen with uncoated steel subjected to chlorides. If the specimen is subjected to carbonation or combination of chlorides and carbonation exposure condition or if the specimen is with inhibitors or coated steel, the equivalent electrical circuit should be chosen accordingly.
- Chloride threshold: The mortar powder from the interface should be collected within 2 mm depth by filing/grinding using dremmel tool and should not go deeper to avoid too much variation in the measured values.

5. Conclusions

The definition of highly resistive (hr) systems based on surface resistivity was established and a new test method for detection of corrosion initiation and determination of chloride threshold (Cl_{th}) of such systems was developed. The steel–cementitious binder (S-B) interface in its microstructural level will have interaction of cement paste and the steel, and the surrounding microclimate determines the corrosion behavior to the larger extent. Hence, the results obtained from the mortar specimens is comparable to that of the concrete specimens [67]. Therefore, the following conclusions were drawn from this experimental work in mortar.

- Any cementitious system irrespective of the binder, binder content, age (at the start of testing), w/b having surface resistivity greater than 37 kΩ.cm is considered as highly resistive cementitious system and the cover resistivity should be accounted for while making data interpretations with respect to corrosion studies.
- A new test method (hr-ACT) is developed for determining Cl_{th} of steel-cementitious systems with high resistivity (ρ > 37 kΩ.cm) subjected to chloride exposure. The time required to determine the Cl_{th} is about 3–4 months. Higher the resistivity of the system, longer will be the test duration.
- As new cementitious materials of high resistivity are coming into the market, hr-ACT developed using EIS technique can be adopted with the chosen equivalent electrical circuit. However, a modification of the circuit is suggested if the system contains advanced construction materials such as corrosion inhibiting admixtures or special type of rebars.
- Cl_{th} of steel is a function of the surrounding cementitious binder. The Cl_{th} of OPC, PC-FA and LC3 was in the order of 0.4, 0.3 and 0.1 percent by weight of binder, respectively. The pH at the S-B interface and buffering capacity reduces due to pozzolanic reaction in highly resistive SCM-based systems and hence reduces the Cl_{th}.
- A lower Cl_{th} does not always means shorter service life. The adverse effects of lower Cl_{th} on service life can be overcome by a lower D_a, which is possible with the use of cements with pozzolanic materials and limestone calcined clay systems.
- One should not select a steel–binder system based on its Cl_{th} *alone*. The synergistic effects of Cl_{th}, D_a, m, and cover depth on the service life must be considered while choosing the steel-binder system.

CRediT authorship contribution statement

Sripriya Rengaraju: Conceptualization, Methodology, Data curation, Visualization, Investigation, Writing – original draft. **Radhakr-**

ishna G. Pillai: Conceptualization, Supervision, Resources, Writing – review & editing.

Declaration of Competing Interest

The authors declare that they have no known competing financial interests or personal relationships that could have appeared to influence the work reported in this paper.

Acknowledgements

This research is partially funded by the Limestone Calcined Clay (LC3) project – Phase I (Project Number: 7F-08527.02.01) sponsored by the Swiss-Agency for Development and Cooperation, Switzerland. The authors also acknowledge the financial support received from the Department of Science and Technology (Sanction No. EMR/2016/003196) and the Ministry of Human Resources Development, Government of India, through Indian Institute of Technology Madras (IITM), Chennai. Also, the authors express their gratitude to the staff and researchers in the Advanced Infrastructure Materials (AIM) Laboratory, Department of Civil Engineering, IITM, Chennai, India.

References

[1] Tutti. Corrosion of Steel in Concrete (Ph.D. Thesis), Lund University, Swedish Cement and Concrete Research Institute, Stockholm. http://portal. research.lu.se/portal/files/4709458/3173290.pdf, Accessed date: 18 July 2018. 1982.
[2] D. Trejo, K. Reinschmidt, Justifying materials selection for reinforced concrete structures. I: Sensitivity analysis, J. Bridge Eng. 12 (1) (2007) 31–37, https://doi.org/10.1061/(ASCE)1084-0702(2007)12:1(31).
[3] U. Angst, B. Elsener, C.K. Larsen, Ø. Vennesland, Critical chloride content in reinforced concrete — A review, Cem. Concr. Res. 39 (12) (2009) 1122–1138.
[4] M.A. Pech-Canul, A.A. Sagüés, P. Castro, Influence of counter electrode positioning on solution resistance in impedance measurements of reinforced concrete, Corrosion 54 (8) (1998) 663–667.
[5] S. Sakir, S.N. Raman, M. Safiuddin, A.B.M. Amrul Kaish, A.A. Mutalib, Utilization of by-products and wastes as supplementary cementitious materials in structural mortar for sustainable construction, Sustainability. 12 (9) (2020).
[6] R.G. Pillai, R. Gettu, M. Santhanam, Use of supplementary cementitious materials (SCMs) in reinforced concrete systems – Benefits and limitations, Revista ALCONPAT 10 (2) (2020) 147–164.
[7] K.M. Smith, A.J. Schokker, P.J. Tikalsky, Performance of supplementary cementitious materials in concrete resistivity and corrosion monitoring evaluations, ACI Mater. J. 101 (5) (2004) 385–390.
[8] C. Alonso, C. Andrade, J.A. González, Relation between resistivity and corrosion rate of reinforcements in carbonated mortar made with several cement types, Cem. Concr. Res. 18 (5) (1988) 687–698.
[9] K. Hornbostel, C.K. Larsen, M.R. Geiker, Relationship between concrete resistivity and corrosion rate - A literature review, Cem. Concr. Compos. 39 (2013) 60–72.
[10] A. Bentur, S. Diamond, N.S. Berke, Steel Corrosion in Concrete: Fundamentals and Civil Engineering Practice, E&FN Spon, London, 1997.
[11] M. Heikal, H. El-Didamony, M.S. Morsy, Limestone-filled pozzolanic cement, Cem. Concr. Res. 30 (11) (2000) 1827–1834.
[12] M.S. Meddah, M.C. Limbachiya, R.K. Dhir, Potential use of binary and composite limestone cements in concrete production, Constr. Build. Mater. 58 (2014) (2014) 193–205.
[13] C.M. Hansson, A. Poursaee, A. Laurent, Macrocell and microcell corrosion of steel in ordinary Portland cement and high performance concretes, Cem. Concr. Res. 36 (11) (2006) 2098–2102.
[14] G. Fajardo, P. Valdez, J. Pacheco, Corrosion of steel rebar embedded in natural pozzolan based mortars exposed to chlorides, Constr. Build. Mater. 23 (2) (2009) 768–774.
[15] D.A. Koleva, J. Hu, A.L.A. Fraaij, K. van Breugel, J.H.W. de Wit, Microstructural analysis of plain and reinforced mortars under chloride-induced deterioration, Cem. Concr. Res. 37 (4) (2007) 604–617.
[16] A. Poursaee, C.M. Hansson, Potential pitfalls in assessing chloride-induced corrosion of steel in concrete, Cem. Concr. Res. 39 (5) (2009) 391–400.
[17] D. Trejo, R.G. Pillai. Accelerated Chloride Threshold Testing: Part I — ASTM A 615 and A 706 Reinforcement, ACI Mater. J. 2003 519–527.
[18] J. Karuppanasamy, R.G. Pillai, A short-term test method to determine the chloride threshold of steel–cementitious systems with corrosion inhibiting admixtures, Mater. Struct. 50 (4) (2017) 1–17.
[19] K. Pettersson. Service life of concrete structures - in a chloride environment. Swedish Cement & Concrete Research Institute, CBI Report 3:96. 1996.
[20] J.J. Kim, Y.M. Young, Study on the passive film of type 316 stainless steel, Int. J. Electrochem. Sci. 8 (10) (2013) 11847–11859.
[21] J.M. Deus, L. Freire, M.F. Montemor, X.R. Nóvoa, The corrosion potential of stainless steel rebars in concrete: Temperature effect, Corros. Sci. 65 (2012) 556–560.
[22] T. Misawa, K. Hashimoto, S. Shimodaira, The mechanism of formation of iron oxide and oxyhydroxides in aqueous solutions at room temperature, Corros. Sci. 14 (2) (1974) 131–149.
[23] C. Andrade, Corrosion of Steel in Concrete Structures, Elsevier, 2016, pp. 269–288, https://doi.org/10.1016/B978-1-78242-381-2.00014-6.
[24] J. Gulikers, R. Polder, M. Raupach, Half-cell potential measurements – Potential mapping on reinforced concrete structures, Mater. Struct. 36 (September) (2003) 1–11.
[25] B. Elsener, Half-cell potential mapping to assess repair work on RC structures, Constr. Build. Mater. 15 (2–3) (2001) 133–139.
[26] M. Pour-Ghaz, O.B. Isgor, P. Ghods, Quantitative Interpretation of Half- Cell Potential, J. Mater. Civ. Eng. 21 (9) (2010) 467–475.
[27] P.C. Andrade, C. Alonso, R. Polder, R. Cigna, O. Vennesland, M. Salta, A. Raharinaivo, B. Elsener. RILEM TC 154-EMC : - Electrochemical Techniques for Measuring Metallic Corrosion Test methods for on-site corrosion rate measurement of steel reinforcement in concrete by means of the polarization resistance method. 37(November 2004) 2005 623–643.
[28] S. Rengaraju, A. Godara, P. Alapati, R.G. Pillai, Macrocell corrosion mechanisms of prestressing strands in various concretes, Mag. Concr. Res. 72 (4) (2020) 194–206.
[29] R.G. Kelly, J.R. Scully, D.W. Shoesmith, R.G. Bucheit, Electrochemical Techniques in Corrosion Science and Engineering, Marcel Dekker Inc, New York, 2003.
[30] F. Mansfeld, The effect of uncompensated IR-drop on polarization resistance measurements, Corrosion 32 (4) (1976) 143–146.
[31] F. Mansfeld, Effect of uncompensated resistance on the true scan rate in potentiodynamic experiments, Corrosion 38 (10) (1982) 556–559.
[32] D.V. Ribeiro, J.C.C. Abrantes, Application of electrochemical impedance spectroscopy (EIS) to monitor the corrosion of reinforced concrete: a new approach, Constr. Build. Mater. 111 (2016) 98–104.
[33] ASTM C876-15 (2015) Standard test method for corrosion potentials of uncoated reinforcing in concrete. ASTM International, West Conshohocken, PA, USA.
[34] ASTM G109-07 (2013) Standard test method for determining effects of chemical admixtures on corrosion of embedded steel reinforcement in concrete exposed to chlorides. ASTM International, West Conshohocken, PA, USA.
[35] ASTM G59-97. (2014). Standard test method for conducting potentiodynamic polarization resistance measurements. ASTM International, West Conshohocken, PA, USA.
[36] ASTM G5 (2014). Standard Reference Test Method for Making Potentiodynamic Anodic Polarization Measurements. ASTM International, West Conshohocken, PA, USA.
[37] ASTM G180-13 (2014). Standard Test Method for Corrosion Inhibiting Admixtures for Steel in Concrete by Polarization Resistance in Cementations Slurries. American Society of Testing and Materials, Conshohocken, PA, USA.
[38] ASTM G102 - 89 Reapproved (2010). Standard Practice for Calculation of Corrosion Rates and Related Information from Electrochemical Measurements. ASTM International, West Conshohocken, PA, USA.
[39] G.S. Frankel, "Electrochemical Techniques in Corrosion: Status, Limitations, and Needs", STP1506 Advances in Electrochemical Techniques for Corrosion Monitoring and Measurement, ASTM International, West Conshohocken, PA, USA, 2009.
[40] S. Chechirlian, M. Keddam, H. Takenouti, Specific Aspects of Impedance Measurements in Low Conductivity Media, in: J.R. Scully, D.C. Silverman, M.W. Kendig (Eds.), Electrochemical Impedance: Analysis and Interpretation, ASTM STP 1188, American Society for Testing and Materials, Philadelphia, 1993, pp. 23–36.
[41] JIS A6205. (2013). Corrosion inhibitor for reinforcing steel in concrete, Japan Industrial standard, 4-1-24, Akasaka, Minato-ku, Tokyo, 107-8440, Japan.
[42] M. Thomas, Chloride Threshold in marine concrete, Cem. Concr. Res. 26 (4) (1996) 513–519.
[43] H.-W. Song, V. Saraswathy, S. Muralidharan, K. Thangavel, Tolerance limit of chloride for steel in blended cement mortar using the cyclic polarisation technique, J. Appl. Electrochem. 38 (4) (2008) 445–450.
[44] D. Izquierdo, C. Alonso, C. Andrade, M. Castellote, Potentiostatic determination of chloride threshold values for rebar depassivation - Experimental and statistical study, Electrochim. Acta 49 (17–18) (2004) 2731–2739.
[45] J. Pacheco, R.B. Polder, Critical chloride concentrations in reinforced concrete specimens with ordinary Portland and blast furnace slag cement, Heron 61 (2) (2016) 99–119.
[46] D.W. Law, J. Cairns, S.G. Millard, J.H. Bungey, Measurement of loss of steel from reinforcing bars in concrete using linear polarisation resistance measurements, NDT E Int. 37 (5) (2004) 381–388.
[47] H.R. Soleymani, M.E. Ismail, Comparing corrosion measurement methods to assess the corrosion activity of laboratory OPC and HPC concrete specimens, Cem. Concr. Res. 34 (2004) (2004) 2037–2044.
[48] C. Andrade, C. Alonso, Corrosion rate monitoring and on-site, Constr. Build. Mater. 10 (5) (1996) 315–328.
[49] RILEM TC 235-CTC (2014), Technical committee Corrosion initiating chloride threshold concentrations in concrete, URL: https://www.rilem.net/groupe/235-ctc-corrosion-initiating-chloride-threshold-concentrations-in-concrete-237. Last accessed on May 19, 2019.
[50] U. Angst, A. Rønnquist, B. Elsener, C.K. Larsen, Ø. Vennesland, Probabilistic considerations on the effect of specimen size on the critical chloride content in reinforced concrete, Corros. Sci. 53 (1) (2011) 177–187.
[51] F. Lollini, E. Redaelli, L. Bertolini, Investigation on the effect of supplementary cementitious materials on the critical chloride threshold of steel in concrete, Mater. Struct. 49 (10) (2016) 4147–4165.
[52] D. Boubitsas, L. Tang, An approach for measurement of chloride threshold values, Int. J. Struct. Eng. 4 (1–2) (2013) 24–34.
[53] R.G. Pillai, Electrochemical characterization and time-variant structural reliability

assessment of post-tensioned, segmental concrete bridges, (Ph.D. dissertation). Texas A&M University, Texas, USA, 2009.
[54] S. Rengaraju, L. Neelakantan, R.G. Pillai, Investigation on the polarization resistance of steel embedded in highly resistive cementitious systems – An attempt and challenges, Electrochim. Acta 308 (2019) 131–141.
[55] SHRP-330 (1993). Standard Test Method for Chloride Content in Concrete Using the Specific Ion Probe, In Condition Evaluation of Concrete Bridges Relative to Reinforcement Corrosion-Volume 8: Procedure Manual, SHRP-S/FR-92-110, Strategic Highway Research Program, Washington, DC, USA, 85-105
[56] ACI, 318–19 Building Code Requirements for Structural Concrete, American Concrete Institute, 2014.
[57] AASHTO T 358 (2017). Standard Method of Test for Surface Resistivity Indication of Concrete's Ability to Resist Chloride Ion Penetration. American Association of State Highway and Transportation Officials, Washington, D.C., U.S.A
[58] A. Malakooti, Investigation of concrete electrical resistivity as a performance based test, M.S. Thesis. Utah state university, Utah, USA, 2017.
[59] Y. Dhandapani, M. Santhanam, Assessment of pore structure evolution in the limestone calcined clay cementitious system and its implications for performance, Cem. Concr. Compos. 84 (2017) 36–47.
[60] B.S. Dhanya, Study of the Influence of Supplementary Cementitious Materials on Selected Durability Parameters of Concrete, Ph.D Thesis. Indian Institute of Technology Madras, Chennai, India, 2015.
[61] J.M.R. Dotto, A.G.de. Abreu, D.C.C. Dal Molin, I.L. Müller, Influence of silica fume addition on concretes physical properties and on corrosion behaviour of reinforcement bars, Cem. Concr. Compos. 26 (1) (2004) 31–39.
[62] S.J. Cooper, A. Bertei, D.P. Finegan, N.P. Brandon, Simulated impedance of diffusion in porous media, Electrochim. Acta 251 (2017) 681–689.
[63] S.N. Victoria, S. Ramanathan, Effect of potential drifts and ac amplitude on the electrochemical impedance spectra, Electrochimica Acta 56 (5) (2011) 2606–2615.
[64] A. Lasia, Electrochemical impedance spectroscopy and its applications, Mod. Aspects Electrochem. 32 (1999) 143–248.
[65] I.-S. Yoon, C.-H. Chang, Effect of chloride on electrical resistivity in carbonated and non-carbonated concrete, Appl. Sci. 10 (18) (2020) 6272, https://doi.org/10.3390/app10186272.
[66] M.G. Fontana, Corrosion Engineering, third ed, McGraw-Hill, Singapore, 1987.
[67] C. Alonso, C. Andrade, M. Castellote, P. Castro, Chloride threshold values to depassivate reinforcing bars embedded in a standardized OPC mortar, Cem. Concr. Res. 30 (7) (2000) 1047–1055.
[68] R.E. Melchers, C.Q. Li, Reinforcement corrosion initiation and activation times in concrete structures exposed to severe marine environments, Cem. Concr. Res. 39 (11) (2009) 1068–1076, https://doi.org/10.1016/j.cemconres.2009.07.003.
[69] RILEM, Draft recommendation for repair strategies for concrete structures damaged by reinforcement corrosion, Materials and Structures 27 (1994) 415–436.
[70] D. Trejo, R.G. Pillai. Accelerated Chloride Threshold Testing : Part I — ASTM A 615 and A 706 Reinforcement. ACI Mater. J. 100 2003 519–527.
[71] C.E. Locke, A. Siman. Corrosion of Reinforcing Steel in Concrete (eds. D.E. Tonini and J.M. Gaidis) p. 3, ASTM STP 713 (1980)
[72] M. Thomas, Chloride thresholds in marine concrete, Cem. Concr. Res. 26 (4) (1996) 513–519, https://doi.org/10.1016/0008-8846(96)00035-X.
[73] D. Trejo, P.J. Monteiro, Corrosion performance of conventional (ASTM A615) and low-alloy (ASTM A706) reinforcing bars embedded in concrete and exposed to chloride environments, Cem. Concr. Res. 35 (3) (2005) 562–571, https://doi.org/10.1016/j.cemconres.2004.06.004.
[74] Life–365. (2012). Service life prediction model and computer program for predicting the service life and life–cycle cost of reinforced concrete exposed to chlorides. URL: http://www.life–365.org/; Last accessed on December 14, 2012.